LCIS: A Boundary Hierarchy For
Detail-Preserving Contrast Reduction

Jack Tumblin and Greg Turk

Georgia Institute of Technology

Abstract

High contrast scenes are difficult to depict on low contrast displays without loss of important fine details and textures. Skilled artists preserve these details by drawing scene contents in coarse-to-fine order using a hierarchy of scene boundaries and shadings. We build a similar hierarchy using multiple instances of a new *low curvature image simplifier* (LCIS), a partial differential equation inspired by anisotropic diffusion. Each LCIS reduces the scene to many smooth regions that are bounded by sharp gradient discontinuities, and a single parameter K chosen for each LCIS controls region size and boundary complexity. With a few chosen K values ($K_1 > K_2 > K_3...$) LCIS makes a set of progressively simpler images, and image differences form a hierarchy of increasingly important details, boundaries and large features.

We construct a high detail, low contrast display image from this hierarchy by compressing only the large features, then adding back all small details. Unlike linear filter hierarchies such as wavelets, filter banks, or image pyramids, LCIS hierarchies do not smooth across scene boundaries, avoiding "halo" artifacts common to previous contrast reducing methods and some tone reproduction operators. We demonstrate LCIS effectiveness on several example images.

CR Descriptors: I.3.3 [**Computer Graphics**]: Picture/image generation - *Display algorithms*; I.4.1 [**Image Processing and Computer Vision**]: Enhancement -*Digitization and Image Capture*

Keywords: Signal Processing, Displays, Non-Realistic Rendering, Level Of Detail Algorithms, Radiosity, Weird Math.

1 Introduction

Local adaptation, the ensemble of local sensitivity-adjusting processes in the visual system, reveals visible details almost everywhere in a viewed scene. Even while driving at night, we see few shadows that are truly featureless black. We can read the tiny lettering on the dazzling surface of a frosted incandescent bulb in a desk lamp, yet we also see the dark room around us. Mechanisms of visual appearance often cause us to underestimate large scene contrasts. For example, we measured a piece of paper on a desk to find it was 1,200 times brighter than the dark carpet in the foot-well

College of Computing, Georgia Institute of Technology,
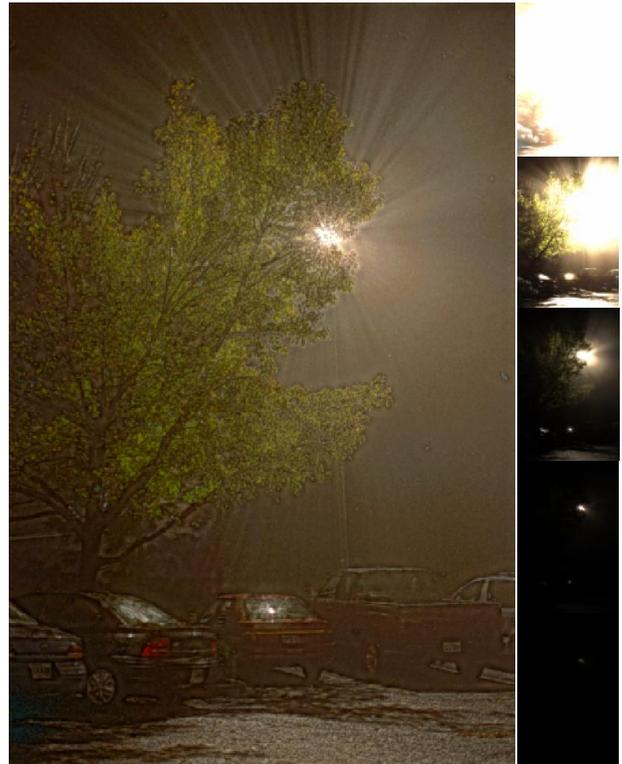Atlanta, GA 30332-0280. ccsupjt@cc.gatech.edu, turk@cc.gatech.edu.

Figure 1: This low contrast image of a streetlight on a foggy night was made by LCIS methods from an extremely high contrast radiance map [2]; Small images show the original scene radiances scaled by progressive factors of 10. Despite scene contrasts greater than 100,000:1, LCIS methods preserve details impossible to capture in a single photograph, including long, dramatic fog streaks, asphalt texture, and tree details in highlight and shadow.

beneath it, yet we could easily see the fibrous textures of both simultaneously. Making an image such as Figure 1 that captures both the high contrast appearance of a scene and its small low-contrast details is contradictory and difficult, and currently the best, most satisfying depictions of these scenes may be the creations of skilled artists.

For three important reasons listed here, cameras and computer graphics renderings have severe difficulties capturing, preserving, and displaying the subtle textures and details in high contrast scenes. First, available display contrasts are small and are easily overwhelmed by the scene contrasts, where contrast is the ratio between two measured light intensities. Newspaper photographs achieve a maximum contrast of about 30:1, typically CRT displays offer contrasts of no more than 100:1, and only the best photographic prints can provide contrasts as high as 1000:1. However, scenes that include visible light sources, deep shadows, and specu-
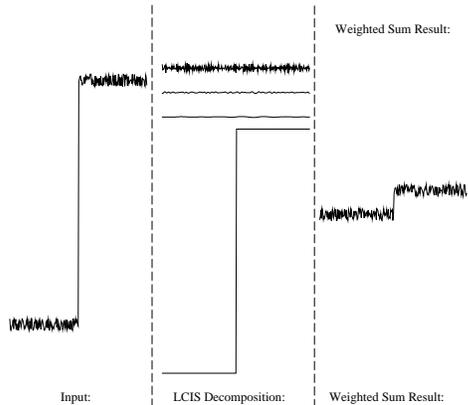
Figure 2: Applied to a scanline from a high contrast scene, an LCIS hierarchy separates large features and fine details as an artist might. Compressing only its simplest features reduces contrasts but preserves details.
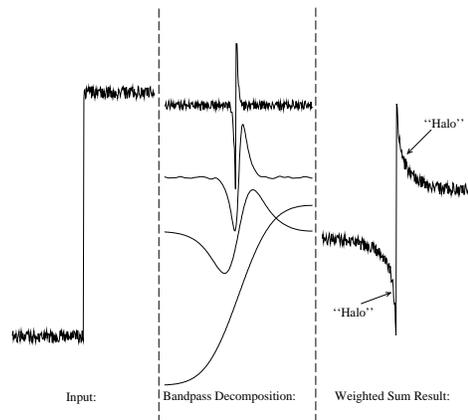

Figure 3: A linear filter hierarchy does not adequately separate fine details from large features. Compressing only the low-frequency components to reduce contrasts causes halo artifacts.

lar highlights can reach contrasts of 100,000:1 or much more.

Second, the simplest ways to adjust scene intensities for display will usually damage or destroy important details and textures. Most commonly used adjustments are borrowed from photography, and are given by

$$I_d = F(m \cdot I_s^\gamma) \qquad (1)$$

where I_d, I_s are display and scene intensities in cd/m^2, m is a scale factor from film exposure, γ is contrast sensitivity and will compress contrasts for values < 1.0, and $F()$ limits the output to display intensity abilities. The simplest, default $F()$ truncates out-of-range intensities to the display limits, but this discards the fine details and textures in the scene's shadows, highlights, or both, depending on "exposure" or scale factor m. Compressing all scene contrasts uniformly by adjusting film gamma γ may compress large contrasts sufficiently for display, but will also reduce smaller contrasts to invisibility. Choosing a better limiting function $F()$ such as the S-shaped response of film can help by gracefully compressing contrasts of scene highlights and shadows, but any function choice forces a tradeoff between preserving details at mid-range and destroying them in shadows and highlights.

Third and most importantly, understanding of the human visual system has not advanced sufficiently to allow construction of a definitive, verifiable, quantitative model of visual appearance, especially for high contrast scenes where local adaptation effects are strong. With these uncertainties, artists offer valuable guidance. Skilled artists learn effective and pleasing ways to convey visual appearance with limited display media, and for some uses their methods are more appropriate than current visual appearance models built from psychophysical measurements and small-signal models. Accordingly, LCIS is an attempt to mathematically mimic a well-known artistic technique for rendering high contrast scenes.

When drawing or painting, many artists capture visual appearance with a "coarse-to-fine" sequence of boundaries and shading. Many begin with a sketch of large, important scene features and then gradually add finer, more subtle details. Initial sketches hold sharply defined boundaries around large, smoothly shaded regions for the largest, highest contrast, and most important scene features. The artist then adds more shadings and boundaries to build up fine details and "fill in" the visually empty regions and capture rich detail everywhere.

This method works particularly well for high contrast scenes because it permits separate contrast adjustments at every stage of increasing detail and refinement. An artist drastically compresses the contrasts of large features, then adds the fine details and textures with little or no attenuation to ensure they are visible in the final image. The artist may also emphasize or mute scene components, to control their prominence and direct the viewer's attention.

An artist's progressive image refinement is quite different from widely used linear filter hierarchies, such as wavelets, filter banks, MIP-maps, and steerable image pyramids. Instead of a hierarchy of sinusoids, artists use a hierarchy of boundaries and shadings. For example, consider a simple high contrast scene made from two adjacent sheets of rough-textured paper. A black-colored sheet on the left is dimly but uniformly lit, but the white sheet on the right is illuminated by a strong white light source sharply masked to fall only on the white paper. To an artist, the scene has only one strong boundary and one faint texture everywhere, as in the scanline plots of Figure 2 (created by LCIS), but to a linear filter decomposition this is a rich, broad-band scene, as in Figure 3. At its largest scale, the linear filter hierarchy is a blurred wash from black to white showing only that the left and right intensities differ greatly. Each finer level contains a strong, zero-mean, ripple-like "detail" that sharpens and narrows the transition from black to white, as if each were improving the focus of a camera. At the finest levels these focus-like "details" overwhelm the much weaker components of the paper texture. Reducing scene contrast by compressing only these coarsest levels fails badly for linear filter methods because some parts of the scene's step-like "large feature" have escaped compression by mixing with fine details of the paper texture. The resulting display image, as shown in Figure 3, suffers from artifacts known variously as "halos" [1], "overshoot-undershoot" or "gradient reversals" [19].

We have devised a new hierarchy that more closely follows artistic methods for scene renderings. Each level of the hierarchy is made from a "simplified" version of original scene made of sharp boundaries and smooth shadings. We named the sharpening and smoothing method "low curvature image simplifiers," or LCIS, and will show in Section 5 how to use it in a hierarchy to convert high contrast scenes to low contrast, highly detailed display images such as Figure 1.

2 Previous Work

Detail-preserving contrast reduction is a small but central part of a broader problem: how can we accurately recreate the visual appearance of all scenes within the narrow limits of existing displays? As discussed by Tumblin and Rushmeier [16], light levels dramatically affect scene appearance; a forest by starlight looks very different in daylight because of complex, light dependent changes in human ability to sense contrast, color, detail, and movement. They advocated "tone reproduction operators" built from mathematical

models of human visual perception to improve displayed images by imitating the light-dependent changes our eyes would experience on viewing the actual scene. We must emphasize that the LCIS method presented here is not true tone reproduction operator, but a sensitive detail extractor for high contrast scenes; it does not determine whether these details would be visible to a human viewer.

Soon afterwards Ward [17] published a simple and practical operator to adjust display brightness by analytically finding scale factor m from scene luminance. Building on this, Ferwerda and colleagues [3] used further psychophysical data to model global adaptation in both cone- and rod-mediated vision, and included changes in sensitivity to color, luminance and spatial resolution in their model. None of these papers have addressed display contrast limitations.

Limited display contrast causes perhaps the worst part of the tone reproduction problem, because most sensations of scene contents, color, acuity, and movements can be directly evoked by the display outputs, but large contrasts cannot. High contrasts must be reduced for display, yet somehow retain a high contrast appearance, perhaps from secondary effects. Papers by Nakamae [7] and Spencer [13] and their colleagues present careful models of the optics of the eye responsible for glare, diffraction, and blooming effects, but as Spencer concluded, these methods must be combined with a perceptually valid method for contrast reduction. Globally applied compression functions (F in Equation 1) such as the S-shaped response of photographic film work well for moderate-contrast scenes, but can easily obliterate details in highlights and shadows. The rational function given by Schlick [12] is an excellent compromise, as it adjusts to keep highlight compression minimal, is fast and simple to compute, and can be calibrated without measuring instruments.

Very large contrasts are much more troublesome because compressive functions destroy important details in highlights and shadows unless adjusted according to local image features. Photographers use "dodging and burning" (moving hand-held masks) to locally adjust print exposure in a darkroom, inspiring an early paper by Chiu *et al.* [1] that constructs a locally varying attenuation factor m by repeatedly clipping and low-pass filtering the scene. Though their method works well in smoothly shaded regions, any small, bright scene feature causes strong attenuation of neighboring pixels and surrounds the feature with a noticeable dark band or halo artifact as in Figure 3. Schlick's attempts to vary his compression function locally also found halos [12], and he suggested local image attenuation should change abruptly at feature boundaries to avoid them. Tanaka and Ohnishi [14] later published a contrast reducing display method similar to Chiu *et al.*, except they used retinal receptive field measurements to design their linear filters. Their method also produces halos. Jobson, Rahman and colleagues [5, 11] devised a contrast reduction method in accordance with Land's "retinex" theory of lightness (perceived reflectance) and color adaptation, but they use linear filters on the logarithm of scene intensities to find local attenuating factors. Their multi-scale extensions help reduce halos by merging results from three manually selected filters.

Ward-Larson *et al.* [19] entirely avoided halos by using iterative histogram adjustment to reduce scene contrasts as part of their tone reproduction operator. Their operator produces very appealing results, and includes locally adjusted models of glare, color sensitivity, and acuity well supported by psychophysical data. However, their computed mapping from scene to display intensities is strictly monotonic, while artists and the LCIS method presented here often use overlapping intensity ranges in different scene regions to achieve greater displayed contrasts for some features. In another halo-free approach, Tumblin and colleagues [15] made computer graphics renderings of separate "layers" of lighting and reflectance and combined them after compressing illumination. They also proposed an interactive display method for high contrast scenes that recomputes the displayed image according to "foveal" neighborhood near the viewer's direction of gaze in the scene.

Building on a rigorous paper on perceptual image metrics [4], last year Pattanaik and colleagues [9] presented a tone reproduction operator that performed contrast reduction using an intricate model of local adaptation assembled from extensive psychophysical data, including acuity, chromatic adaptation, and many measured non-linearities of vision. However, contrast reduction is chiefly due to attenuation in a linear filter hierarchy; despite many admirable qualities, their method is still susceptible to strong halo components.

3 LCIS Method: Shocks and Smoothing

The central importance of boundaries and shadings in artistic renderings suggests a new image decomposition method. To an artist, shadings usually refer to regions of nearly uniform intensity gradient. Because the gradients change smoothly and gradually with position, the region has low curvature. An image made entirely of low curvature regions has boundaries defined by gradient discontinuities, and these may include both ridge-like and step-like features, but only ridges are necessary, as a step may be regarded as two adjacent ridge-like features.

The intensities and locations of these boundaries alone are sufficient to construct an interesting form of simplified image by interpolating between the boundaries with a curvature-minimizing process. The result has an interesting physical analogy; imagine image boundary intensities as a height field made from a frame of thin wires. Dipping the wires in soapy water forms low-curvature bubble membranes between the wires. By adding more wires we may encode the entire scene by boundaries and their intensities. Such an artist-like coarse-to-fine hierarchy is possible if we create a well-behaved method to find these boundaries and smooth away their intervening details.

Anisotropic diffusion has shown great success as a boundary-finding intra-region smoothing method [10] and gathered widespread attention in the image processing literature. Mathematically, it is a gradual, time-dependent evolution of an image towards a piecewise-constant approximation, as shown in Figure 5. The change in image intensity over time is determined by the same class of partial differential equations (PDEs) that govern diffusion of heat or other fluids through solids. For example, if we regard the image intensity $I(x, y)$ as the temperature of a large flat plate of uniform thin material, and also treat temperature as a measure of heat fluid per unit area, then the change in I over time is given by:

$$I_t = \nabla \cdot (-\mathbf{\Phi}) = \nabla \cdot (C \nabla I) \qquad (2)$$

Subscripts denote partial derivatives such that I_t is $(\partial/\partial t)I(x, y, t)$, the time rate of change in temperature, I_x is $(\partial/\partial x)I(x, y, t)$, I_{xx} is $(\partial^2/\partial x^2)I(x, y, t)$, and so forth. C is the heat conductance scalar, and $\mathbf{\Phi}$ is the heat flux, the velocity vector for heat fluid.

In this classic heat equation, heat flows "downhill" from hot regions to cold regions, from larger I to smaller I, as permitted by material conductance C; $0 \leq C \leq 1$, and all heat fluid movements are described by their flux vector $\mathbf{\Phi}$. The flux is caused by a "motive force" pushing the fluid in the hot-to-cold direction given by the negative gradient vector $-\nabla I = (I_x, I_y)$, and by the material's conductance C. If conductance is a constant, C_0, the equation reduces to $I_t = C_0(I_{xx} + I_{yy})$; as time passes the image changes in the same way it would if repeatedly convolved with a Gaussian filter kernel, smoothing away differences between neighboring points and asymptotically approaching a uniform temperature. The conductance C determines how fast this smoothing occurs, and if C is constant the behavior is known as isotropic diffusion.

In anisotropic diffusion the conductance depends on the image, and both the image and the conductance evolve over time in more interesting ways. In their seminal 1990 paper, Perona and Malik [10] noted that conductance controls the rate of local image
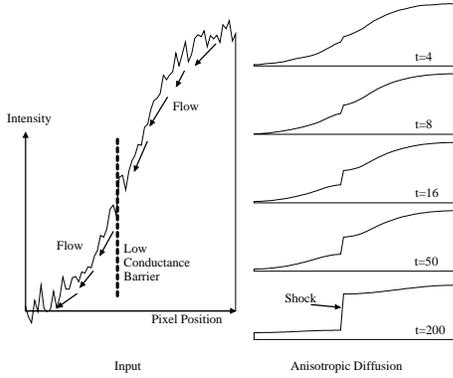
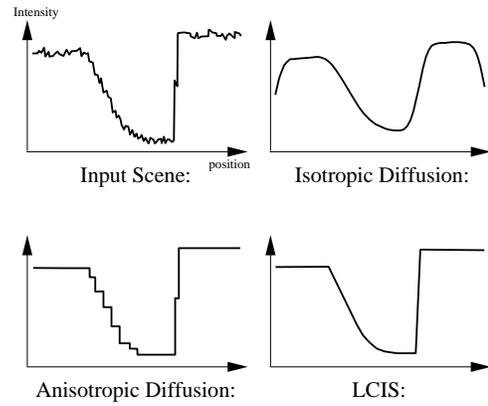Figure 4: Anisotropic diffusion rapidly forms step discontinuities or "shocks" in high gradient regions.

Figure 5: Isotropic diffusion uniformly smoothes the entire image; anisotropic diffusion forms step-like shocks at persistent high gradients and smoothes away all intensity variations between them, sometimes forming "stair-steps" [20]; but LCIS forms ridge-like shocks at persistent high curvatures and smoothes away the gradient variations between them.

smoothing, and proposed that conductance should vary inversely with a local "edginess" estimate to find, preserve, and sharpen image edges. This edginess value is a measure of the likelihood that a point is near an edge or boundary. Low conductance at likely edge locations and high conductances elsewhere preserves 'edgy' features, yet rapidly smoothes away the details and textures between them, and simple edginess estimates work well. They used gradient magnitude scalar $\|\nabla I\|$ and offered two inverse functions to find variable conductance $C(x, y, t)$. Thus anisotropic diffusion is:

$$
\begin{aligned}
I_t &= \nabla \cdot (C(x, y, t)\nabla I) & (3)\\
&= \frac{\partial}{\partial x}(CI_x) + \frac{\partial}{\partial y}(CI_y) & (4)
\end{aligned}
$$

where $C(x, y, t) = g\left(\|\nabla I\|\right) = g\left(\sqrt{I_x^2 + I_y^2}\right)$, and (chosen from Perona and Malik [10]):

$$
g(m) = \frac{1}{1 + \left(\frac{m}{K}\right)^2}, \qquad (5)
$$

where K is the "conductance threshold" for m.

Anisotropic diffusion is especially interesting because both its edge-preserving and its smoothing abilities are self-reinforcing, as illustrated in Figure 4. Small-gradient regions have high conductance, allowing easy fluid flow that further reduces gradients. Large-gradient regions have low conductance, discouraging flow as if forming a weak barrier. However, higher conductances of its surroundings let fluid erode and steepen the already large gradients. Heat fluid seeps inwards towards the "uphill" side of the barrier, and fluid quickly drains away from the "downhill" side, making the large gradient region narrower and steeper, strengthening its barrier effect. The region quickly evolves into a step-wise discontinuity with infinite gradient and zero conductance known as a "shock.". As a result, anisotropic diffusion transforms an image into a piecewise constant approximation with step-like discontinuities in regions of high 'edginess'.

More importantly, the self-reinforcing behaviors of anisotropic diffusion improve its performance as a boundary finder. Gradient magnitudes much larger than the "gradient threshold" K in Equation 5 will consistently form shocks, but the boundary/not-boundary decision is not a simple threshold testing process. Image behavior at points where gradient magnitude is near K is strongly influenced by image surroundings; gradients less than K may still form shocks if another shock is forming nearby, and small, isolated fine details with gradients greater than K are still smoothed away. Thus anisotropic diffusion finds boundaries according to both their

gradients and their surroundings, sharpens the boundaries to create shocks, and smoothes away all textures and details between them.

Though numerically stable and guaranteed to converge to a piecewise-constant solution as $t \to \infty$, Nitzberg and Shiota [8] and others have shown that anisotropic diffusion is ill-posed; infinitesimal changes in input can cause very large changes in output due to the shock-forming process. Shocks usually form at local gradient maxima and follow image boundaries closely, but this is not always true. Regions of high, approximately uniform gradient may develop shocks anywhere within the region. Instead of a single large, centrally placed shock, anisotropic diffusion may develop multiple shocks placed seemingly at random, causing "stairsteps" in the region as shown in Figure 4 and explored by Whitaker and Pizer [20].

Inspired by anisotropic diffusion, we have created a related set of PDEs that capture its self-reinforced smoothing and shock-forming behavior, but is driven by higher derivatives of the image I. Instead of evolving an image towards a piecewise constant approximation by driving all gradients towards zero or infinity, our equations smooth and sharpen an image towards a piecewise linear approximation by driving all curvatures towards zero or infinity. Because boundary conditions usually prevent a zero curvature solution, we call our method a "low curvature image simplifier"(LCIS).

As with anisotropic diffusion, LCIS equations describe fluid flow, but both the motive force pushing the fluid and the variable conductances permitting flow are computed differently. The "motive force" of anisotropic diffusion is the negative gradient $-\nabla I$, but LCIS pushes fluids to encourage uniform gradients; it pushes outwards from intensity peaks or ridges with negative curvature and inwards towards pits or hollows with positive curvature. Therefore the LCIS motive force vector should follow positive derivatives of curvature, but these form a tensor with no obvious single direction. Instead, we define the motive force vector using simpler directional derivatives and vector integration. To evaluate the motive force at image point $I(x_0, y_0)$, we first define a 1-D line L through the point with orientation θ and signed distance parameter α along line L. We evaluate the image I along line L and find its third derivative $I_{\alpha\alpha\alpha}$ as a measure of curvature change in the direction given by θ:

$$
\begin{aligned}
A &= x_0 + \alpha\cos\theta, & (6)\\
B &= y_0 + \alpha\sin\theta. & (7)\\
I_\alpha(A, B) &= I_x(A, B)\cos\theta + I_y(A, B)\sin\theta
\end{aligned}
$$

$$= \left(\left(\frac{\partial}{\partial x} \right) \cdot \cos\theta + \left(\frac{\partial}{\partial y} \right) \cdot \sin\theta \right) I. \quad (8)$$

$$I_{\alpha\alpha} = \left(\left(\frac{\partial}{\partial x} \right) \cdot \cos\theta + \left(\frac{\partial}{\partial y} \right) \cdot \sin\theta \right)^3 I, \quad (9)$$

where (A, B) are (x, y) coordinates of line $L(\alpha)$, I_α is the directional derivative of I along line L, and $I_{\alpha\alpha\alpha}$ is the third derivative of I along line L.

If $I_{\alpha\alpha\alpha} > 0$, then the curvature $I_{\alpha\alpha}$ is increasing along line L as it passes through point (x_0, y_0); flow in that direction would help equalize curvatures on either side of the point and reduce $I_{\alpha\alpha\alpha}$. Accordingly, we let $I_{\alpha\alpha\alpha}$ define the strength of an infinitesimal motive force vector along line L, and we sum up these tiny forces for all orientations θ to find the force vector's x and y components, labeled "East" and "North" to avoid confusion with partial derivatives, and given by: $\mathbf{F} = (f_E, f_N)$;

$$f_E = \frac{1}{\pi} \int_0^{2\pi} I_{\alpha\alpha\alpha} \cos\theta \, d\theta = \frac{3}{4}(I_{xxx} + I_{yyx}), \quad (10)$$

$$f_N = \frac{1}{\pi} \int_0^{2\pi} I_{\alpha\alpha\alpha} \sin\theta \, d\theta = \frac{3}{4}(I_{xxy} + I_{yyy}). \quad (11)$$

For LCIS conductance, we use Equation 5 from anisotropic diffusion, but now the m argument is given by a new "edginess" estimate. As our desired ridge-like shocks have infinite curvature, we construct m from a non-directional measure of curvature magnitude: $m^2 = 0.5(I_{xx}^2 + I_{yy}^2) + I_{xy}^2$. Our "low curvature image simplifier" is then defined as:

$$I_t(x, y, t) = \nabla \cdot (C(x, y, t) \mathbf{F}(x, y, t)) \quad (12)$$

where $\mathbf{F}(x, y, t)$ is the motive force vector computed from partial derivatives and given by $\mathbf{F} = (f_E, f_N) = (I_{xxx} + I_{yyx}, I_{xxy} + I_{yyy})$, and conductance $C(x, y, t) = g(m)$ is computed from "edginess" m using Equation 5.

Low curvature image simplifiers (LCIS) share several important properties with anisotropic diffusion. Equation 12 is adiabatic; intensity neither created nor destroyed. LCIS meets the goals set forth by Perona and Malik [10]; varying its conductance threshold K defines a continuous scale space that exhibits causality, immediate localization, and piecewise smoothing. Conductance is inversely linked with the motive force, causing rapid shock formation at image boundaries, and smoothing between boundaries is self-reinforcing, though asymptotic. Unlike anisotropic diffusion, LCIS shocks are discontinuities in gradient instead of intensity; they form ridge-like features that appear step-like when adjacent. Just as large high gradient regions can cause multiple shocks or "stairstepping" in anisotropic diffusion results, LCIS can also form multiple shocks unpredictably in large regions of uniform high curvature. However, high curvature regions tend to be smaller due to the larger intensity range they require, and we have found that multiple ridge-like shocks are far less visually apparent than stairsteps. Finally, both anisotropic diffusion and LCIS are formally defined for continuously variable (x, y). Any practical implementations must use discrete approximations.

4   LCIS Implementation

Our pixel-based LCIS approximation is straightforward to implement. We use explicit integration with a fixed timestep to find $I(t)$, compute a new image on each timestep, assume constant conductance and flux during each timestep, and compute flux only between 4-connected neighboring pixels. The computation is entirely local; each new image is computed only from pixels in the previous timestep's image, and each new pixel is computed from a fixed set of neighboring pixels in the previous image.
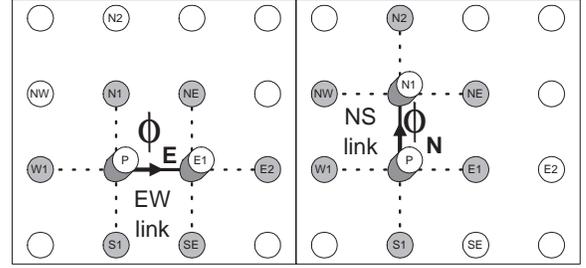

Figure 6: LCIS transfers intensity through "links" between pixels. On each timestep, flux ϕ_E, ϕ_N flows through EW and NS links respectively, computed from the gray-shaded pixels.

Continuing with the fluid flow analogy, imagine that each pixel is a tank holding a fluid volume equal to the pixel intensity. Each pixel reservoir is tied to each of its four-connected neighbors through separate pipelines or "links." As shown in Figure 6, pixel P has links to pixels $E1$, $N1$, $W1$, and $S1$. During a fixed timestep T we transfer a fluid quantity "flux" ϕ through a link, decreasing the source pixel intensity and increasing the destination. On each timestep we compute flux for each link and then adjust the current image by the flux amounts to create a new output image.

The left and right sides of Figure 6 show the two types of links. The drawing on the left shows an EW link connecting pixels P and $E1$. The flux ϕ_E that flows through this EW link is computed from the values of eight neighborhood pixels shown in gray and connected by dotted lines. The sign of ϕ determines flow direction: $\phi_E > 0$ flows in the $+x$ direction, which lowers the intensity of pixel P and increases pixel $E1$ by the same amount. Similarly, link NS connects pixels P and $N1$, and positive flux ϕ_N flows in $+y$ direction to diminish P and increase $N1$.

Motive force through each link is found from forward-difference estimates of third partial derivatives of the image at each link center. For the EW link between pixels P and $E1$:

$$I_{xxx} = (E2 - W1) + 3(P - E1), \quad (13)$$
$$I_{yyx} = (NE - N1) + (SE - S1) + 2(P - E1), \quad (14)$$

and for the NS link between P to $N1$,

$$I_{yyy} = (N2 - S1) + 3(P - N1), \quad (15)$$
$$I_{xxy} = (NE - E1) + (NW - W1) + 2(P - N1). \quad (16)$$

Conductance of each link is found from forward difference estimates of second partial derivatives. We define:

$$P_{xx} = E1 + W1 - 2P, \qquad P_{yy} = N1 + S1 - 2P,$$
$$E_{xx} = E2 + P - 2E1, \qquad E_{yy} = NE + SE - 2E1,$$
$$N_{xx} = NE + NW - 2N1, \quad N_{yy} = N2 + P - 2N1,$$

and

$$N_{xy} = (NE - E1) - (N1 - P),$$
$$S_{xy} = (E1 - SE) - (P - S1),$$
$$W_{xy} = (N1 - P) - (NW - W1).$$

The square of our edginess estimate m is:

$$m_{EW}^2 = (P_{xx}^2 + P_{yy}^2 + E_{xx}^2 + E_{yy}^2)/4 +$$
$$(N_{xy}^2 + S_{xy}^2)/2 \text{ for EW links, and} \quad (17)$$

$$m_{NS}^2 = (P_{xx}^2 + P_{yy}^2 + N_{xx}^2 + N_{yy}^2)/4 +$$
$$(W_{xy}^2 + N_{xy}^2)/2 \text{ for NS links.} \quad (18)$$

Assuming constant curvatures and flow rates during each timestep, the flux through each link is the product of timestep length, motive force, and conductance, given by $\phi_E = TF_E C_E$ and $\phi_N = TF_N C_N$. We recommend a timestep of $T \leq 1/32$ for stability. F_E and F_N are the motive forces driving EW and NS flux, given by $F_E = (I_{xxx} + I_{yyx})$ and $F_N = (I_{xxy} + I_{yyy})$. Conductances through NS and EW links are

$$C_E = \frac{1}{1 + \left(\frac{m_{EW} D_E}{K}\right)^2} \qquad (19)$$

and

$$C_N = \frac{1}{1 + \left(\frac{m_{NS} D_N}{K}\right)^2}. \qquad (20)$$

where m_{EW}, m_{NS} are edginess estimates from Equations 17 and 18, D_E, D_N are leakfix multipliers explained below, initialized to 1.0.

Estimating image derivatives with adjacent pixel differences causes "leakage" problems. Shocks in continuous images form perfectly impermeable boundaries to prevent any fluid flow across them. Though discrete images also form shocks, neither the gradients nor the curvature estimates reach infinity due to the fixed, finite spacing between pixels, allowing small fluid flows or "leaks" across boundaries that should be impermeable. Small leaks over many timesteps gradually erode the image boundaries and eventually destroy them all. Though several papers (*e.g.* [6]) offer strategies for stopping the time evolution before boundary erosion is too large, any chosen stopping time is a compromise between adequate intra-region smoothing and minimal leakage. Instead, we devised a simple leakage fix that works quite well for both discrete LCIS and anisotropic diffusion.

Our leakage fix is a single self-adjusting "leakfix multiplier" value D_E or D_N stored for each EW or NS link respectively and used in Equations 19 and 20. We noticed in Equation 5 that shock forming drives all the edginess estimates m rapidly away from the conductance threshold K in the earliest timesteps. Edginess estimates at boundaries are boosted towards infinity by shock formation, and self-reinforced smoothing drives all other m below K and towards zero. To identify and prevent leakage as an image evolves, we continually compare m against K to find links that cross image boundaries and should hold shocks, and we adjust D_E or D_N of these links to amplify their edginess estimates m and drive conductance towards zero. Leakfix multipliers grow exponentially with time in links where m is consistently larger than K, but settles rapidly back towards 1.0 if edginess falls below K. In our implementation, initially $D_E = 1.0$ and $D_N = 1.0$ for all pixels, then for each timestep:

$$D_E = \begin{cases} D_E(1.0 + m_{EW}) & \text{if}(m_{EW} > K), \\ 0.9D_E + 0.1 & \text{otherwise, and} \end{cases} \qquad (21)$$

$$D_N = \begin{cases} D_N(1.0 + m_{NS}) & \text{if}(m_{NS} > K), \\ 0.9D_N + 0.1 & \text{otherwise.} \end{cases} \qquad (22)$$

The leakage fix also provides a convenient marker for boundaries; we label any link with a leakfix multiplier greater than 10.0 as a "boundary link" that may cross a ridge-like boundary shock in the image. Even though conductance drops to zero at LCIS shocks, our analysis of continuous LCIS showed ridge-like shocks should not evolve into step-like shocks during intra-region smoothing. To prevent this divergence in our discrete implementation, we also mark the pixels on either end of a boundary link as "boundary pixels" and stop all subsequent flux into or out of these pixels; see the Proceedings CD-ROM for source code. With this simple two-part fix we have not encountered any noticeable problems with leakage or boundary erosion.
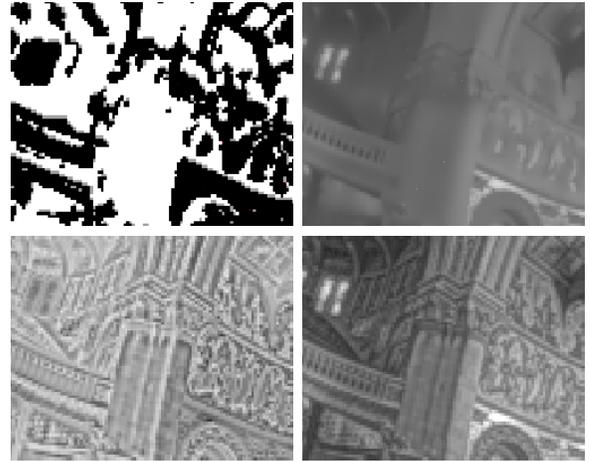

Figure 7: Images from an LCIS hierarchy reveal its methods. From a part of the church scene of Figure 9, LCIS creates a boundary pixel map (top left), and a simplified image (top right), shown after contrast compression to make it displayable. A detail image (lower left) holds the input minus the simplified image. A detailed displayable image(lower right) is the sum of images at upper right and lower left.
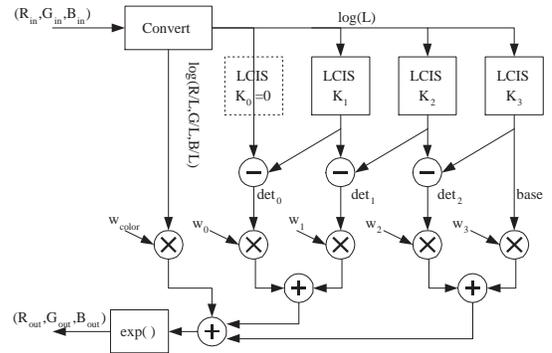

Figure 8: Detail-preserving contrast reduction method using an LCIS hierarchy, as used for Figures 1 and 9.

5 Contrast Reduction: LCIS Hierarchy

Discrete LCIS mimics the artist's drawing process in reverse; it selectively removes details from a scene to leave only smoothly shaded regions separated by sharp boundaries. We can easily recover the removed details by subtracting the LCIS-smoothed image from the original scene, and then follow the artists scheme for detail-preserving contrast reduction: we strongly compress the contrasts of the simplified image, then add in the details with little or no compression, as shown in Figure 7.

The LCIS hierarchy shown in Figure 8 shows the expandable multiscale form we used to make Figures 1 and 9. Just as an artist may create an image by progressive refinement, the LCIS hierarchy extracts preserved scene details with a progressive set of LCIS settings. We first convert the scene to its base-10 logarithm so that pixel differences directly correspond to contrasts (intensity ratios). Our handling of color here is rudimentary: we apply LCIS only to scene luminances and reconstruct color outputs using color ratios as suggested by Schlick [12]. Next, we make a set of progressively simpler images by applying LCIS with progressively larger K values starting from zero: when $K = 0$, LCIS has no effect on the
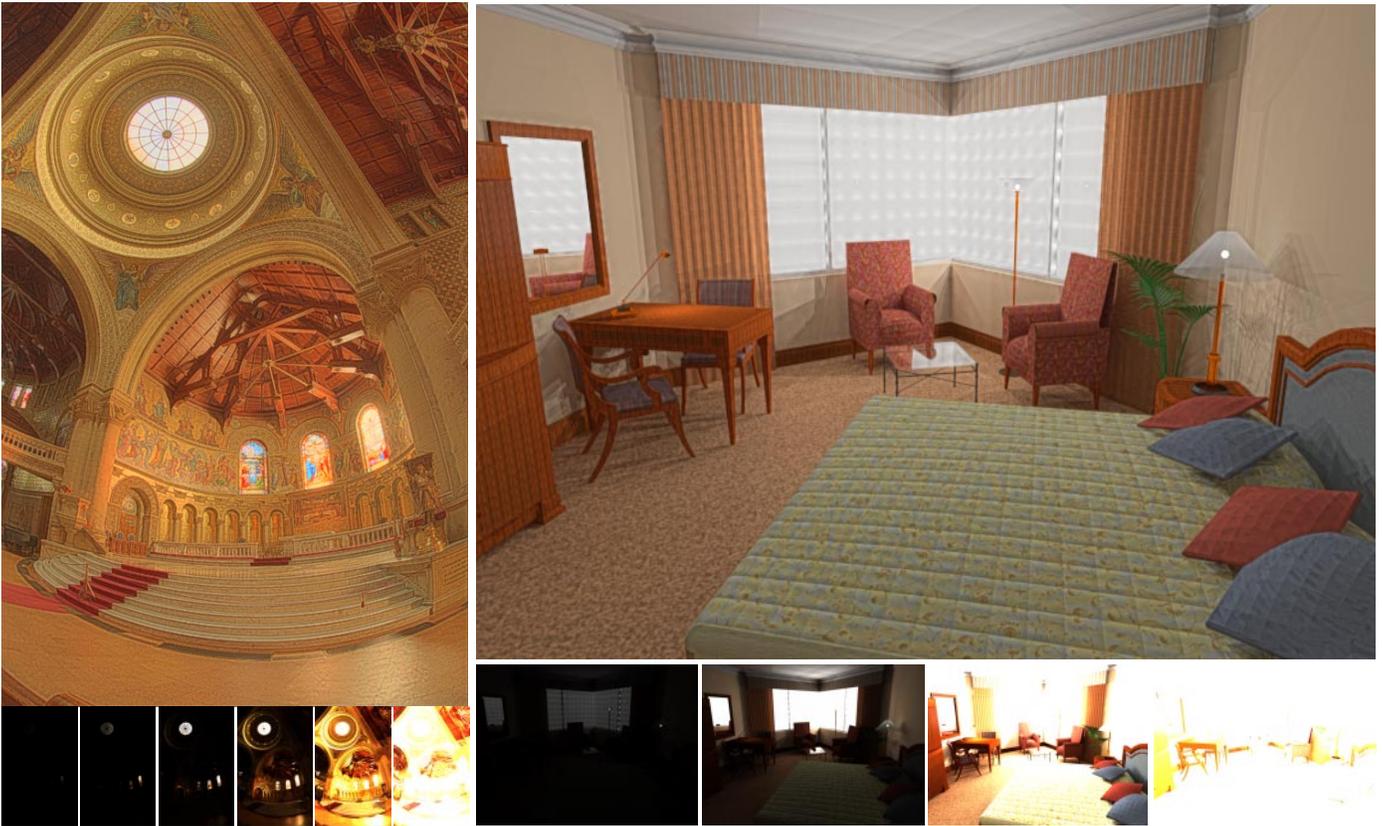
Figure 9: These low contrast, highly detailed display images were made using an LCIS hierarchy as diagrammed in Figure 8. In the Stanford Memorial Church scene (radiance map courtesy Paul Debevec, University of California at Berkeley; see [2]), note the visible floor tile seams, wood grain, gold inlay texture, and stone arch fluting. Vast contrasts ($> 250,000 : 1$) prevent capturing all these details within a single photograph. The hotel room image, from a radiometrically accurate high contrast scene ($> 70,000 : 1$) designed and rendered by Simon Crone using RADIANCE [18], shows rich detail everywhere, even in highlights and shadows; note the floor lamp bulb and glass shade still plainly visible against the brilliant window shades, and the complex shadows on the wall and ceiling. Source Image: Proposed Burswood Hotel Suite Refurbishment (1995). Interior Design – The Marsh Partnership, Perth, Australia. Computer Simulation – Lighting Images, Perth, Australia. Copyright © 1995 Simon Crone.

input image. For the church scene in Figure 9 we used $K_1 = 0.06$, $K_2 = 0.10$ and $K_3 = 0.16$. LCIS with the largest K value makes the simplest or "base" image, and we extract a graduated set of "detail" images ($det_0, det_1, ...$) by subtraction, with the finest details in det_0. Next, we compress their contrasts by scaling (for the church image in Figure 9 we chose $w_{0,1,2,3} = 1.0, 0.8, 0.4, 0.16$, $w_{color} = w_3$) and then add and exponentiate to find display intensities. Our test-bed software allows us to interactively adjust the parameters K, w, and the number of LCIS timesteps, and by trial and error we found 100 to 1000 timesteps and K from 0.02 to 0.32 spanned our entire range of interest for all our test scenes. Though w_{base} is dictated by desired display contrast, w_0 is usually best around 1.0 with intervening w values between the two, none are critical; a wide range of settings provides a pleasing visual appearance and small changes are not easy to notice. Usually $w_{color} = w_{base}$ looked pleasant, but some images looked better with exaggerated values: we set $w_{base} = 0.2$ in the hotel room scene, but used $w_{color} = 0.6$ to avoid a "washed out" appearance.

6   Results

As shown in Figures 1 and 9, the LCIS hierarchy reveals an astonishing amount of subtle detail and scene content. Though we think the histogram-based result of Ward-Larson *et al.* [19] (also

seen in [2]) is a more beautiful and natural-looking depiction of Debevec's Stanford Church radiance map, it does not include many features clearly visible in the LCIS result. For example, note the intricate gold filigree in the ceiling dome. Linear filter-based methods have difficulties with strong halo artifacts cause by the skylight nearby. LCIS also reveals rich detail in the hotel room scene; previous depictions of this scene often made the carpet and bed covering look muted and subtle, here we see strong wood, bedspread and carpet textures. The elaborate shadow details behind the plant and on the ceiling also suggests the sun and sky lighting was approximated with several point sources.

We confirmed that these details exist at these contrasts in the scene by using simple scaling and truncation to display scene radiances. In Figures 1 and 9 we include tiny versions of scaled, truncated scene radiances with $\gamma = 1.0$ and scale factor m (Equation 1) increasing by a factor of 10 for each successive image to help viewers understand the scenes' huge contrasts.

Computing costs for LCIS results are moderate in our current implementation. Written in Visual C++ without regard for speed or efficiency, using 32-bit floating point values for all images and computations, our code required 14 minutes 47 seconds to compute a 187x282-pixel image of Figure 1 on a 200 MHz Pentium Pro with 128MB RAM running Windows NT4.0. This timing result includes five LCIS simplifiers computing 500 timesteps each, the auxiliary calculations diagrammed in Figure 8, and windowing and display

overhead of an interactive data-flow application. Most of our tests of LCIS behavior and our choices of parameters such as curvature thresholds K, weighting factors w, and the number of timesteps were made interactively on much smaller images (often 128 x 192) where computing delays rarely exceeded 30 seconds. We found that parameter choices at low resolutions invariably worked well for much larger images, and no parameter settings needed extensive or critical tuning. Better integration methods and software tuning may also greatly improve these initial LCIS speed ratings.

7 Discussion and Future Work

LCIS smoothing and LCIS hierarchies offer a new way to decompose an image reversibly into a multiscale set of large features, boundaries and fine details. It permits a novel form of detail-preserving contrast reduction that avoids halo artifacts common to previous methods based on linear filtering. Detail extraction problems arise in many domains, and LCIS may also be useful for viewing other high contrast signals such as data from astronomy, radiology or seismology. The initial results images presented here are promising, but our LCIS work has many open questions and opportunities for further research. Though we found the K and w controls of the LCIS hierarchy easy to use, they affect the image globally; would localized, paint-box-like controls to vary them within the scene be a useful artistic tool? Conversely, how could we best apply psychophysical data to control an LCIS hierarchy automatically and perform as a true tone reproduction operator? How could a more thoughtful treatment of color better exploit the boundary and detail information it contains?

We have also discovered that even though LCIS forms sharp boundaries without smoothing across them, sometimes weak, "residual halo" artifacts can appear with strong contrast reductions. However, even the worst residual halos are far weaker than those from linear filters, and are caused by a different mechanism. Residual halos seem to form only in blurred image regions with high contrast, sparse shocks and low curvature such as a badly out-of-focus step image. If shocks do not form at the blurred boundary, LCIS further smoothes the region and reduces its curvature, causing a broad low-curvature component to appear in one or more "detail" images in Figure 8. Weak residual halos are visible in Figure 1 under the left lowermost tree branches. We are currently investigating a solution for this anomaly.

We do not yet fully understand the relationship between curvature, spatial scale, contrast, and shock formation for a given K, but suspect that the extensive published studies of anisotropic diffusion may offer help. Large scale, high contrast scene features such as soft shadows may have very low curvatures obscured by small scale high curvature textures; can LCIS-like methods find shocks for both? Can we ensure "reasonable" behavior for LCIS for all possible images?

Finally, extending LCIS to higher dimensions appears straightforward, and may be useful for revealing fine details in high contrast 3D scalar and vector fields or for motion estimation in high contrast scenes.

8 Acknowledgements

References

[1] K. Chiu, M. Herf, P. Shirley, S. Swamy, C. Wang, and K. Zimmerman. Spatially nonuniform scaling functions for high contrast images. In *Proceedings of Graphics Interface '93*, pages 245–254, May 1993.

[2] P. E. Debevec and J. Malik. Recovering high dynamic range radiance maps from photographs. In *SIGGRAPH 97*, pages 369–378, August 1997.

[3] James. A. Ferwerda, Sumant N. Pattanaik, Peter Shirley, and Donald P. Greenberg. A model of visual adaptation for realistic image synthesis. In Holly Rushmeier, editor, *SIGGRAPH 96*, Annual Conference Series, pages 249–258, August 1996.

[4] James A. Ferwerda, Sumanta N. Pattanaik, Peter Shirley, and Donald P. Greenberg. A model of visual masking for computer graphics. In Turner Whitted, editor, *SIGGRAPH 97*, Annual Conference Series, pages 143–152, August 1997.

[5] D. J. Jobson, Z. Rahman, and G. A. Woodell. A multiscale retinex for bridging the gap between color images and the human observation of scenes. *IEEE Transactions on Image Processing*, 6(7):965–976, July 1997.

[6] X. Li and T. Chen. Nonlinear diffusion with multiple edginess thresholds. *Pattern Recognition*, 27(8):1029–1037, August 1994. Pergamon Press.

[7] E. Nakamae, K. Kaneda, T. Okamoto, and T. Nishita. A lighting model aiming at drive simulators. In *Computer Graphics (SIGGRAPH 90 Conference Proceedings)*, Annual Conference Series, pages 395–404, August 1990.

[8] M. Nitzberg and T. Shiota. Nonlinear image filtering with edge and corner enhancement. *IEEE Transactions on Pattern Analysis and Machine Intelligence*, 14(8):826–833, August 1992.

[9] Sumanta N. Pattanaik, James A. Ferwerda, Mark D. Fairchild, and Donald P. Greenberg. A multiscale model of adaptation and spatial vision for realistic image display. In Michael Cohen, editor, *SIGGRAPH 98*, Annual Conference Series, pages 287–298, July 1998.

[10] P. Perona and J. Malik. Scale-space and edge detection using anisotropic diffusion. *IEEE Transactions on Pattern Analysis and Machine Intelligence*, 12(7):629–639, July 1990.

[11] Z. Rahman, D. J. Jobson, and G. A. Woodell. Multi-scale retinex for color image enhancement. In *Proceedings, International Conference on Image Processing*, volume 3, pages 1003–1006, June 1996. Held in Lausanne, Switzerland 16-19 September 1996.

[12] C. Schlick. Quantization techniques for visualization of high dynamic range pictures. In G. Sakas, P. Shirley, and S. Mueller, editors, *Photorealistic Rendering Techniques*, Proceedings of the 5th Eurographics Rendering Workshop 13-15 June 1994, pages 7–20, Berlin, 1995. Springer Verlag.

[13] G. Spencer, P. Shirley, K. Zimmerman, and D. P. Greenberg. Physically-based glare effects for digital images. In *SIGGRAPH 95*, Annual Conference Series, pages 325–334, August 1995.

[14] T. Tanaka and N. Ohnishi. Painting-like image emphasis based on human vision systems. In D. Fellner and L Szirmay-Kalos, editors, *EUROGRAPHICS '97*, volume 16(3), pages C253–C260. The Eurographics Association, 1997.

[15] J. Tumblin, J. Hodgins, and B. Guenter. Two methods for display of high contrast images. *ACM Transactions On Graphics*, 18(1):(to appear), January 1999.

[16] J. Tumblin and H. Rushmeier. Tone reproduction for computer generated images. *IEEE Computer Graphics and Applications*, 13(6):42–48, November 1993.

[17] G. Ward. A contrast-based scalefactor for luminance display. In Paul S. Heckbert, editor, *Graphics Gems IV*, chapter Frame Buffer Techniques: VII.2, pages 415–421. AP Professional, Cambridge MA 02139, 1994.

[18] G. Ward. The RADIANCE Lighting simulation and rendering system. In *SIGGRAPH 94*, Annual Conference Series, pages 459–472, July 1994.

[19] G. Ward Larson, H. Rushmeier, and C. Piatko. A visibility matching tone reproduction operator for high dynamic range scenes. *IEEE Transactions on Visualization and Computer Graphics*, 3(4):291–306, October-December 1997.

[20] R. Whitaker and S Pizer. A multi-scale approach to nonuniform diffusion. *CVGIP: Image Understanding*, 57(1):99–110, January 1993.